The impact of pressure and temperature on growth rate and layer uniformity in the sublimation growth of AlN crystals

Gao, Bing
Research Institute for Applied Mechanics, Kyushu University

Nakano, Satoshi
Research Institute for Applied Mechanics, Kyushu University

Kakimoto, Koichi
Research Institute for Applied Mechanics, Kyushu University

出版情報：Journal of Crystal Growth. 338 (1), pp.69-74, 2012-01-01. Elsevier
バージョン：

The impact of pressure and temperature on growth rate and layer uniformity in the sublimation growth of AlN crystals

B. Gao, S. Nakano, K. Kakimoto

Research Institute for Applied Mechanics, Kyushu University, Kasuga, Fukuoka 816-8580, Japan

Email: gaobing@riam.kyushu-u.ac.jp

Tel) 81-92-583-7744

Fax) 81-92-583-7743

Keywords: A1. Computer simulation; A1. Heat transfer; A1. Substrate; A2. Growth from vapor

PACS: 02.60.Cb; 44.10. +i; 44.40. +a

Abstract

To effectively design a large furnace for producing large-size AlN crystals, a fully coupled compressible flow solver was developed to study the sublimation and mass transport processes in AlN crystal growth. Compressible effect, buoyancy effects, flow coupling between aluminum gas and nitrogen gas, and Stefan effect are included. Two sets of experimental data were used to validate the present solver. Simulation results showed that the distributions of Al and N_2 partial pressures are opposite along the axial direction due to constant total pressure and Stefan effect, with the Al and nitrogen partial pressures being highest at the source and seed crystals positions, respectively. The distributions of species inside the growth chamber are obviously two-dimensional, which can curve a flat crystal surface. Simulation results also showed that AlN crystal growth rate can be increased by reducing total pressure or by increasing seed temperature or by increasing source-seed temperature difference. High nitrogen pressure causes decrease in growth rate, but it is beneficial for obtaining uniform growth rate in the radial direction. Results of simulation also showed that there is an optimized temperature difference (40°C) in the present furnace for obtaining good homogeneity of growth rate.

1. Introduction

AlN is an attractive candidate for electronic, optical and opto-electronic applications due to its high electrical resistivity, high thermal conductivity, large band gap, high acoustic wave velocity and excellent lattice and thermal expansion match with GaN [1,2]. Bulk AlN crystals are commonly grown by the physical vapor transport (PVT) method [3-6]. In bulk AlN growth, there are still some unresolved problems that limit commercial utilization of the material. One of them is related to crystal size. Large crystal size imposes stringent requirements on the choice and control of operating conditions, and the cost for an individual growth run is high [7]. Large crystal size is also a challenge for maintaining high quality [8]. Therefore, to effectively increase crystal size and maintain high quality, accurate global numerical simulation for a large furnace should first be implemented from growth system design to optimization of growth conditions. Many numerical simulations of AlN sublimation growth have been done [9-15], and the results of those simulations have contributed to mechanism analysis and control optimization of an AlN sublimation growth system.

We have developed a fully coupled compressible flow solver that includes almost all of the effects in AlN sublimation growth, such as effects of compressibility, buoyancy and flow coupling between aluminum gas and nitrogen gas, Stefan effect, and surface kinetics effect. Evaporation and deposition flux is automatically provided according to the supersaturation of species at the seed or supercooling at the powder source. Therefore, this set of analysis systems has a strong ability to predict the process of AlN crystal growth.

2 Numerical simulations of heat and mass transport

2.1 Configurations of the furnace

For preliminary studies, a large experimental growth furnace was used to validate our numerical results. For configurations of the furnace, refer to the paper [16]. The AlN PVT growth system consists of AlN powder, a graphite crucible, an insulation shield, a graphite pedestal and induction coils. The AlN powder is placed inside the crucible, and the seed is attached to the bottom of the lid of the crucible. The diameter of the seed is $50\ mm$ and the distance between the source and seed surface is about 45 mm. The furnace is assumed to be axisymmetric. An extra annular-square chamber is connected to the top of the main growth chamber by a small gap. The gap can be adjusted from 0.1 mm to 3.0 mm.

2.2 Global heat transfer

Our simulation implementation involves two steps: first, the temperature distribution of furnace components due to heat transfer and heat radiation is computed without gas flow, and then the flow field and temperature field inside the gas part are computed using the temperature boundary conditions from the first step.

Global modeling of heat transfer in the furnace involves induction heating by an electromagnetic field, conductive heat transfer in all solid components, and radiation heat transfer in all enclosures. The radiative heat exchange is modeled on the basis of the assumption of diffuse-gray surface radiation [17]. For the present initial stage, a steady-state process is assumed. The calculation starts when both of the gas reactions above the source and seed surfaces reach equilibrium states. That state is called as an initial stage. Global simulation of heat transfer shows that the temperatures are about $2329\,K$ at the center of the powder face and about $2270\,K$ at the center of the seed face.

2.3 Mass transport

For a fully coupled compressible flow for mixed species written in general curvilinear coordinates, refer to the paper [18]. The boundary conditions of temperature at the source and seed faces are set to values computed from the global heat transfer. The velocities at the source and seed faces are provided according to the definition of Stefan velocity. The velocity at the crucible surface is set to zero.

In the present calculation, two main species, Al and N_2 [9-15], are taken in the gas part for the sublimation and deposition processes. It is assumed that there are no homogeneous chemical reactions in the vapor phase. Heterogeneous chemical reactions occur at the crystal and source faces.

As pointed out in the paper [19], there is a thin Knudsen layer on the source face or on the seed face, the phase of which is between solid and vapor. Vapor flux at the source and seed faces can be exactly determined by the Hertz-Knudsen equation. Conceptually, that relation may be treated as a kinetic jump of vapor pressure at the Knudsen layer [19]. Inside the two thin Knudsen layers, the Hertz-Knudsen equation is used to calculate the sublimation and deposition mass flux at the seed face and the source face. For example, at the seed face, the deposition molar flux is given by

$$(\chi_i \vec{V} - D_i \nabla \chi_i) \cdot \vec{n} = \gamma_i \frac{1}{\sqrt{2\pi M_i \Re T}} (p_i - p_i^*), i = 1, 2, \qquad (1)$$

where χ_i is the molar concentration of species i, $\vec{V}$ is the Stefan velocity, and γ_i is the sticking coefficient of species i, which is taken from the paper [5]; $\vec{n}$ is the unit normal vector of the surface, which is consistent with the direction of molar flux; M_i is the molecular weight of species i, $\Re$ is the universal gas constant, and p_i^* is the equilibrium pressure of species i. We use the indexes 1 and 2 to denote Al and N_2, respectively.

Attention must be paid to the equilibrium pressure in Eq. (1). For AlN sublimation growth, the following reaction on the source surface is considered: $AlN(s) \rightarrow Al(g) + \frac{1}{2} N_2(g)$. Two different cases are discussed for this reaction. The first case is gas pressure being zero before any chemical reaction occurs inside the growth chamber. When the sublimation reaction occurs and it finally reaches an equilibrium, the equilibrium pressure of species can be approximately obtained from the paper [20]. The second case is gas pressure being much larger than zero before any chemical reaction occurs inside the growth chamber because of an excess of nitrogen gas in the furnace. When the sublimation reaction occurs, the chemical reaction to the right side will be markedly suppressed by the high nitrogen pressure. This is equivalent to the way of filling excess of nitrogen gas into the equilibrium state of the first case, which causes the chemical reaction to move to the left side until reaching a new equilibrium. At the new equilibrium state, the aluminum pressure in the second case will become smaller than that in the first case. Therefore, the equilibrium pressure of species in the furnace is dependent on both the temperature and nitrogen pressure.

To effectively model the dependency of equilibrium pressure on nitrogen pressure, we introduce the concept of equilibrium total pressure. Due to the extremely low flow velocity in the furnace, total pressure in the growth cell remains almost constant. We can set the equilibrium total pressure P_{total}^{*} as

$$P_{total}^{*} = P_{Al}^{*} + P_{N_2}^{*} = P_{total}, \tag{2}$$

where P_{Al}^{*} and $P_{N_2}^{*}$ are the equilibrium pressures of aluminum and nitrogen gases, respectively, and P_{total} is the actual total pressure in the furnace.

The equilibrium pressures of nitrogen and aluminum gases should also satisfy the

mass action law:

$$P_{Al}^{*} P_{N_2}^{*\,1/2} = K_{eq}, \tag{3}$$

where K_{eq} is the equilibrium constant, which is a function of temperature and can be calculated using standard thermodynamic properties of the species involved.

Therefore, the new equilibrium pressures of nitrogen and aluminum gases, which are dependent on temperature and total pressure, can be solved from Eqs. (2) and (3).

If the equation of state is used, the relationship between pressure and molar concentration of species can be written as

$$p_i = \chi_i \Re T, i = 1, 2. \tag{4}$$

If Eq. (4) is substituted into Eq. (1), there are still three unknowns, which are χ_1, χ_2 and $\vec{V}$. However, only two equations are available. To close the system and make the solution unique, an extra boundary condition at the deposition layer is needed. As pointed out by Francesconi [21], total pressure is uniform throughout the deposition layer for Stefan flow. We introduce the following boundary condition:

$$\nabla p_{total} = 0. \tag{5}$$

For the curvilinear seed face, we set the tangential velocity to zero, i.e.,

$$\vec{V} \cdot \vec{\tau} = 0. \tag{6}$$

For the basic iteration procedure for solving the seed boundary conditions, refer to the paper [8]. For the source boundary conditions, almost the same procedure can be implemented.

3. Validation of present solver

For validation of the present solver, two sets of experimental data were used. One set of data is from Liu and Edgar [13] and the other set is from Wolfson and Mokhov

[12]. The geometrical parameters of the present furnace were adjusted according to their experimental furnaces. The boundary conditions for the present mass transport calculations were taken as their corresponding experimental conditions.

In the first experiment [13], seed temperature, temperature gradient and source-seed distance were 2123.15 K, 3.5 K/mm, and 9 mm, respectively. In this paper, temperature gradient is defined by the ratio of source-seed temperature difference to source-seed distance. Growth pressure was changed from 10 Torr to 800 Torr. Growth rate comparison between numerical and experimental data is shown in Fig. 1. It can be seen that the present numerical results are almost the same as the experimental results over a very wide pressure range, indicting that the present solver has good ability to predict correct growth rate.

In the second experiment [12], seed temperature, temperature gradient and source-seed distance were 2273.15 K, 7 K/mm, and 3 mm, respectively. In the experiment, growth rate was measured by the increase in weight of the substrate, rather than from that in the layer thickness [12]. Thus, the measured growth rate only denotes an average value. The average growth rate might be smaller than the local growth rate at the center of seed due to the large inhomogeneity of growth rate distribution especially in a low pressure system. For the present calculation, the value of the growth rate is taken at the center of the seed. Growth rate comparison between numerical and experimental data is already shown in Fig. 1. It can be seen that in a low pressure condition, a slightly higher growth rate than the experimental data is obtained by the present solver. However, the tendency of variation in growth rate with an increase in pressure is correctly obtained by the present numerical solver.

3 Results of computation

3.1 Two-dimensional characteristics

3.1.1 Distributions of Al and N_2 gases

One simulation was done using seed temperature of 2270 K, temperature gradient of 1.31 K/mm, source-seed distance of 45 mm, and furnace total pressure of 700 Torr. The distributions of Al species (left side) and N_2 species (right side) are shown in Fig. 2. It can be seen that Al pressure is high near the source and that it gradually decreases from the source to the seed. However, the N_2 gas exhibits a distribution opposite to that of Al gas. The N_2 pressure is low near the source and gradually increases from the source to the seed.

The distribution of Al gas is valid since the Al gas first evaporates from the source and then flows toward to the seed, finally depositing on the seed surface. For the distribution of N_2 gas, some explanations are needed since N_2 gas also evaporates from the source first. From the point of view of constant total pressure, N_2 pressure at the source surface is surely small since Al pressure there is high. From the point of view of the Stefan effect and flow coupling between Al gas and N_2 gas, the global Stefan flow carries N_2 gas from the source to the seed, but only a small portion of the N_2 gas is incorporated into the AlN crystal and more and more N_2 gas is accumulated near the seed surface, causing a back-diffusion of N_2 gas from the seed to the source. The convection transport of N_2 gas from the source to the seed is almost balanced by the back-diffusion from the seed to the source. Therefore, the gradual decrease of Al pressure and the gradual increase of N_2 pressure from the source to the seed are valid distributions.

3.1.2 Two-dimensional influences on crystal growth

Two-dimensional effects are important and can lead to radially varying growth

rates. The two dimensionality of species distribution is obvious in Fig. 2. Good homogeneity can be obtained only near the central axis of the furnace. The inhomogeneity is unavoidable due to the temperature inhomogeneity. For the same growth conditions as those in Fig. 2, the growth rate distribution at the initial stage along the seed surface is shown in Fig. 3. It can be seen that the crystal growth rate is not uniform along the seed. From the edge of the seed to the center, the growth rate increases from zero to a maximum value and then decreases to an almost constant value. Thus, the initial shape of the crystal interface will approach a two-peak curve, which is consistent with results of SiC PVT growth modeling [23]. Therefore, the two dimensionality of mass transport has a large effect on evolution of the shape of the AlN crystal interface.

3.2 Effects of growth conditions on AlN crystal growth

3.2.1 Pressure effect

The value of total pressure in the furnace has an obvious effect on crystal growth, as has been pointed out in many papers [3,12,13]. The results of calculation shown in Fig. 1 clearly indicate that the growth rate can be markedly reduced by an increase in total pressure. There are two reasons for the obvious decrease in growth rate when pressure increases. One reason is that the sublimation process is suppressed by high-pressure nitrogen gas in the furnace, which causes an obvious decrease in aluminum gas pressure, and the other reason is that the transport of aluminum gas from the source to the seed is also suppressed by the high-pressure nitrogen gas.

Attention should be paid to the pressure effect on growth homogeneity. Figure 4 (a) shows the growth rate distribution along the seed at different pressures. It can be seen that when pressure increases, the distribution of growth rate along the seed becomes

more homogenous. For a description of the pressure effect on growth homogeneity in a more quantitative manner, the ratios between the maximum and minimum growth rates at different pressures are shown in Figure 4 (b). It can be seen that when the pressure increases, the ratio is close to one, which means that the growth rate distribution is homogeneous. Therefore, high pressure can produce a flat crystal surface, although it clearly decreases growth rate.

3.2 Seed temperature effect

Seed temperature has a great effect on growth rate. To clarify the effect of seed temperature, calculations were implemented with different seed temperatures and with other parameters fixed. In the calculations, gas total pressure, temperature gradient and source-seed distance were 350 Torr, 1.11 K/mm and 45 mm, respectively. Growth rates with different seed temperatures are shown in Fig. 5. It can be seen that growth rate increases rapidly with increase in seed temperature. The reason for the dependency of growth rate on seed temperature needs to be illuminated since all of the other parameters, including gas pressure, source-seed distance and source-seed temperature difference, were fixed. As is well known [13], the equilibrium pressure difference between the source and the seed is a critical parameter for growth rate. Figure 6 shows equilibrium pressure differences in aluminum gas between the source and the seed with different seed temperatures. Comparing the results shown in Fig. 5 with those shown in Fig. 6, it can be seen that the two figures exhibit similar tendencies when seed temperature increases. Therefore, the effect of seed temperature on growth rate is mainly due to the faster increase in equilibrium pressure at the source than that at the seed.

3.3 Source-seed temperature difference effect

The source-seed temperature difference plays an essential role in determining growth rate. Numerical experiments were also done by changing only the source-seed temperature difference and fixing other parameters. In the calculations, gas total pressure, seed temperature and source-seed distance were 425 Torr, 2270 K and 45 mm, respectively. Thus, only source temperatures were changed in the calculations. The results for growth rate as a function of radius of a crystal are shown in Fig. 7. Although the growth rate is very small due to the very high gas pressure, it can be seen that when the source-seed temperature difference increases from 10 K to 80 K, the growth rate increases by almost 4.2 times. Therefore, a good method for increasing growth rate is to increase the source-seed temperature difference.

However, large-sized AlN crystal growth requires a homogenous growth rate along the seed face for high quality. It is essential to observe the growth rate distribution variation along the seed when the source-seed temperature difference changes. Figure 8 shows growth rate variations near the edge and near the center with different temperature differences. The results show that an optimized temperature difference, which is close to 40 K in the present furnace, can be obtained because there the growth rate exhibits good homogeneity due to equal growth rates near the edge and near the center.

4. Conclusions

A fully coupled compressible flow solver was used to study the sublimation and mass transport processes during AlN crystal growth. Comparison of numerical and experimental data showed that growth rate can be correctly obtained by using the present solver.

The results of simulation showed that the distributions of Al and N_2 partial pressures in the furnace were opposite along the axial direction, with the Al and N_2 partial pressures being highest at the source and seed crystal positions, respectively. The distribution of species is obviously two-dimensional, which can curve a flat crystal surface. Results of simulation also showed that AlN crystal growth rate can be increased by reducing total pressure or by increasing seed temperature or by increasing source-seed temperature difference. High nitrogen pressure causes decrease in growth rate, but it is beneficial for obtaining uniform growth rate in the radial direction. Results of simulation also showed that there is an optimized temperature difference (40°C) in the present furnace for obtaining good homogeneity of growth rate.

Acknowledgments

We acknowledge professor Nobuyuki Imaishi and Dr. Shin-ichi Nishizawa for his fruitful discussions.

References

[1] J.C. Rojo, L.J. Schowalter, R. Gaska, M. Shur, M.A. Khan, J. Yang, D.D. Doleske, J. Cryst. Growth 240 (2002) 508.

[2] B. Wu, H. Zhang, Int. J. Heat Mass Transfer, 47 (2004) 2989.

[3] S.Yu. Karpov, D.V. Zimina, Yu.N. Makarov, E.N. Mokhov, A.D. Roenkov, M.G. Ramm, Yu.A. Vodakov, Phys. Stat. Sol. (a) 176 (1999) 435.

[4] E.N. Mokhov, O.V. Avdeev, I.S. Barash, T.Yu. Chemekova, A.D. Roenkov, A.S. Segal, A.A. Wolfson, Yu.N. Makarov, M.G. Ramm, H. Helava, J. Cryst. Growth 281 (2005) 93.

[5] Yu.N. Makarov, O.V. Avdeev, I.S. Barash, D.S. Bazarevskiy, T.Yu. Chemekova, E.N. Mokhov, S.S. Nagalyuk, A.D. Roenkov, A.S. Segal, Yu.A. Vodakov, M.G. Ramm, S. Davis, G. Huminic, H. Helava, J. Cryst. Growth 310 (2008) 881.

[5] S.Yu. Karpov, A.V. Kulik, A.S. Segal, M.S. Ramm, Yu.N. Makarov, phys. stat. sol. (a) 188 (2001) 763.

[6] B. Wu, R. Ma, H. Zhang, M. Dudley, R. Schlesser, Z. Sitar, J. Cryst. Growth 250 (2003) 14.

[7] M.V. Bogdanov, S.E. Demina, S.Yu. Karpov, A.V. Kulik, M.S. Ramm, Yu. N. Makarov, Cryst. Res. Technol. 38 (2003) 237.

[8] B. Gao, X.J. Chen, S. Nakano, S. Nishizawa, K. Kakimoto, J. Cryst. Growth 312 (2010) 3349.

[9] B. Wu, R. Ma, H. Zhang, V. Prasad, J. Cryst. Growth 266 (2004) 303.

[10]D. Cai, L.L. Zheng, H. Zhang, V.L. Tassev, D.F. Bliss, J. Cryst. Growth 293

(2006) 136.

[11] L. Liu, J.H. Edgar, J. Cryst. Growth 220 (2000) 243.

[12] A.A. Wolfson, E.N. Mokhov, Semiconductors 44 (2010) 1383.

[13] L. Liu, J.H. Edgar, J. Electrochem. Soc. 149(1) (2002) G12.

[14] S.Yu. Karpov, A.V. Kulik, A.S. Segal, M.S. Ramm, Yu.N. Makarov, Phys. Stat. Sol. (a) 188 (2001) 763.

[15]A.S. Segal, S.Yu. Karpov, Yu.N. Makarov, E.N. Mokhov, A.D. Roenkov, M.G.Ramm, Yu.A.Vodakov, J. Cryst. Growth 211 (2000) 68.

[16] X. J. Chen, L. J. Liu, H. Tezuka, Y. Usuki, K. Kakimoto, J. Cryst. Growth 310 (2008) 1810.

[17] F. Dupret, P. Nicodeme, Y. Ryckmans, P. Wouters, M. J. Crochet, Int. J. Heat Mass Transfer, 33 (1990) 1849.

[18] J. S. Shun, K. H. Chen, Y. Choi, J. Comput. Phys., 106 (1993) 306.

[19] A. S. Segal, A. N. Vorob'ev, S. Yu. Karpov, Yu. N. Makarov, E. N. Mokhov, M. G. Ramm, M. S. Ramm, A. D. Roenkov, Yu. A. Vodakov, A.I. Zhmakin, Mater. Sci. Eng., B 61-62 (1999) 40.

[20] G.A. Slack, T.F. Mcnelly, J. Cryst. Growth 34 (1976) 263.

[21] R. Francesconi, Chem. Eng. J. 16 (1978) 101.

[22] P.M. Dryburgh, J. Cryst. Growth 125 (1992) 65.

[23] S.Yu. Karpov, A.V. Kulik, I.A. Zhmakin, Yu.N. Makarov, E.N. Mokhov, M.G. Ramm, M.S. Ramm, A.D. Roenkov, Yu.A. Vodakov, J. Cryst. Growth 211 (2000) 347.

Figure captions

Fig. 1. Growth rate comparison between numerical and experimental data for one case of seed temperature of 2123.15 K, source-seed distance of 9 mm, and temperature gradient of 3.5 K/mm and for another case of seed temperature of 2273.15 K, source-seed distance of 3 mm, and temperature gradient of 7 K/mm.

Fig. 2. Distributions of Al species (left side) and N_2 species (right side) for seed temperature of 2270 K, source-seed distance of 45 mm, temperature gradient of 1.31 K/mm, and gas pressure of 700 Torr.

Fig. 3. Growth rate distribution along the seed surface for the same conditions as those in Fig. 2.

Fig. 4. (a) Growth rate distribution along the seed with different pressures for seed temperature of 2270 K, source-seed distance of 45 mm, and temperature gradient of 1.31 K/mm, (b) Ratios of maximum growth rate to minimum growth rate with different pressures.

Fig. 5. Growth rate variation with different seed temperatures for source-seed distance of 45 mm, temperature gradient of 1.11 K/mm, and gas pressure of 350 Torr.

Fig. 6. Equilibrium pressure difference of aluminum gas between the source and the seed with different seed temperatures for the same conditions as those in Fig. 5.

Fig. 7. Growth rate distribution along the seed with different source-seed temperature difference for seed temperature of 2270 K, source-seed distance of 45 mm, and gas pressure of 425 Torr.

Fig. 8. Growth rate variation near the edge and near the center with different

source-seed temperature differences for the same conditons as those in Fig. 7.

Fig. 1.

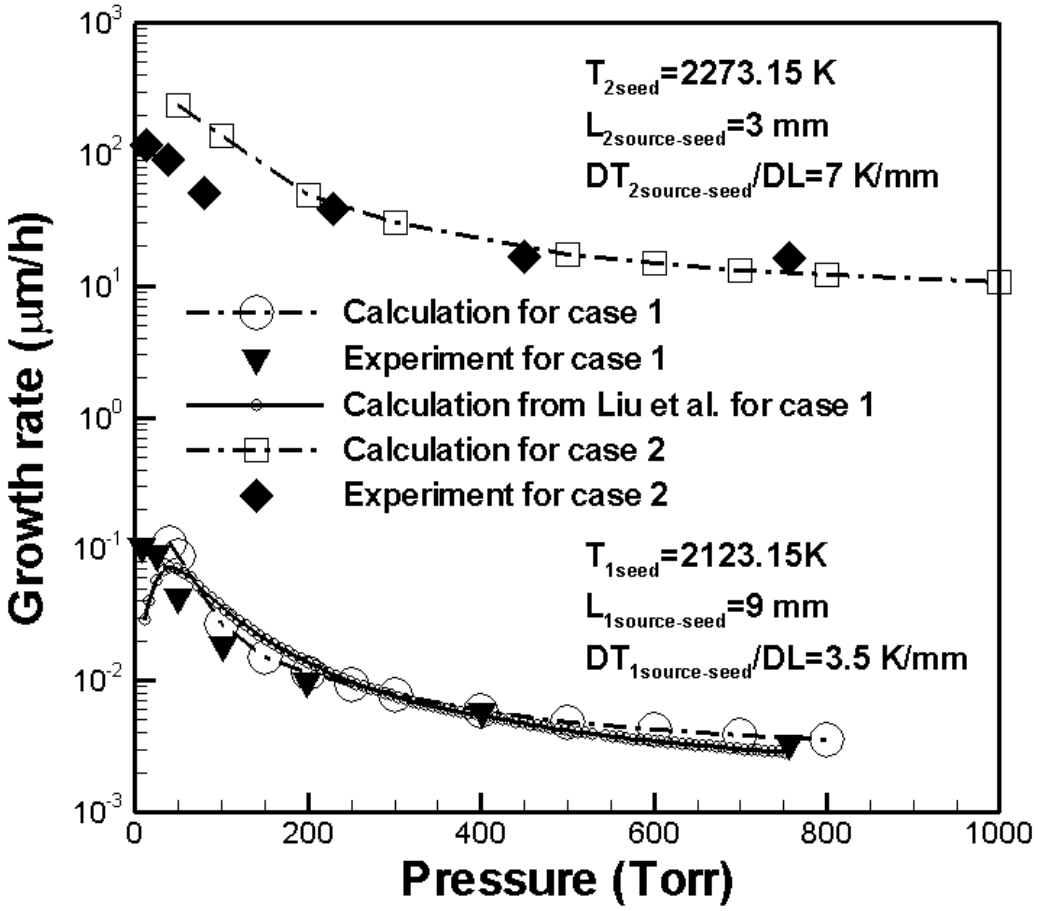
T_{2seed}=2273.15 K
$L_{2source-seed}$=3 mm
$DT_{2source-seed}$/DL=7 K/mm
Calculation for case 1
Experiment for case 1
Calculation from Liu et al. for case 1
Calculation for case 2
Experiment for case 2
T_{1seed}=2123.15K
$L_{1source-seed}$=9 mm
$DT_{1source-seed}$/DL=3.5 K/mm
Growth rate (μm/h)
Pressure (Torr)
10^3
10^2
10^1
10^0
10^{-1}
10^{-2}
10^{-3}
0
200
400
600
800
1000

Fig. 2.

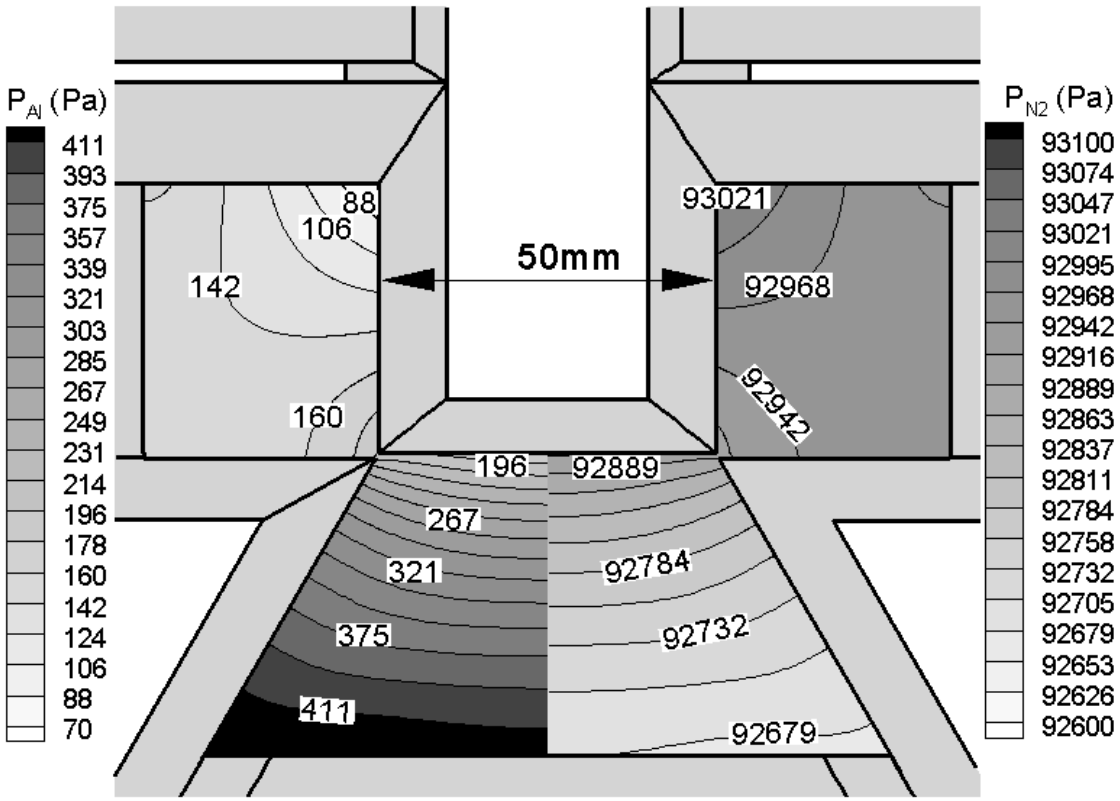
P_Al (Pa)
411
393
375
357
339
321
303
285
267
249
231
214
196
178
160
142
124
106
88
70
P_N2 (Pa)
93100
93074
93047
93021
92995
92968
92942
92916
92889
92863
92837
92811
92784
92758
92732
92705
92679
92653
92626
92600
50mm
88
106
142
160
196
267
321
375
411
93021
92968
92942
92889
92784
92732
92679

Fig. 3.

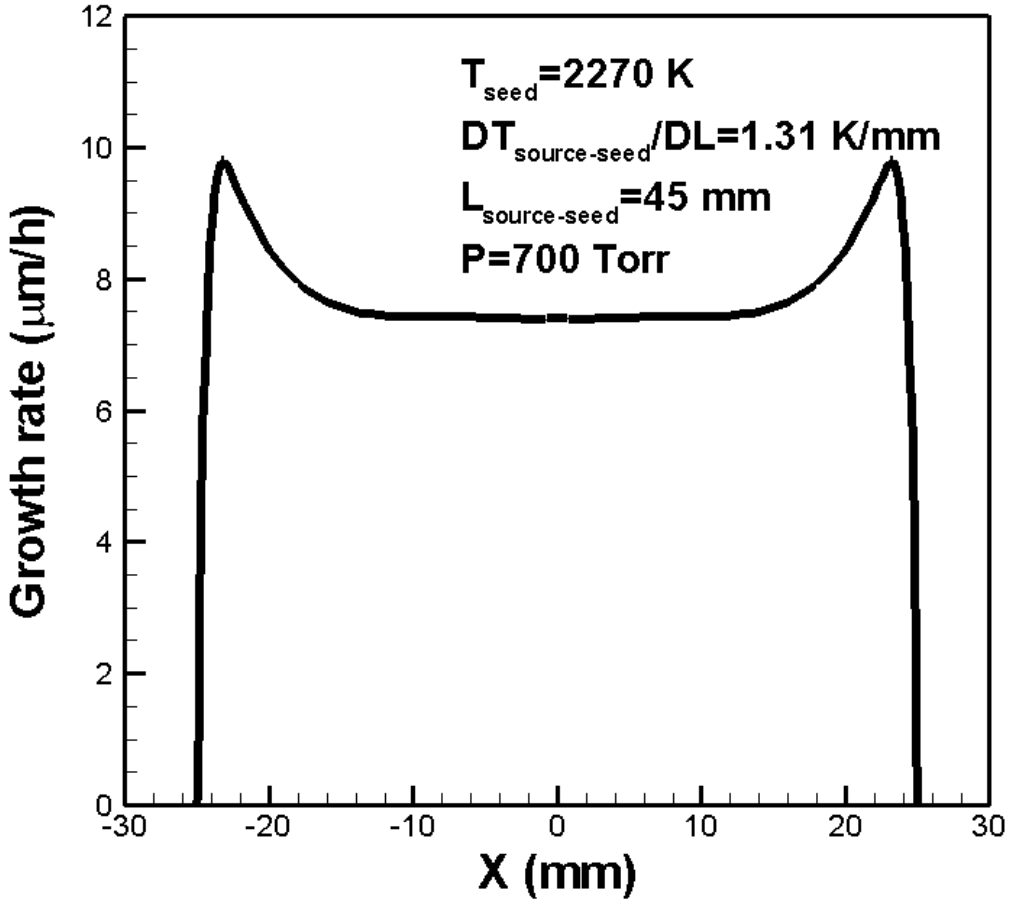
T_{seed}=2270 K
$DT_{source-seed}$/DL=1.31 K/mm
$L_{source-seed}$=45 mm
P=700 Torr
Growth rate (μm/h)
X (mm)
0
2
4
6
8
10
12
-30
-20
-10
0
10
20
30

Fig. 4(a).

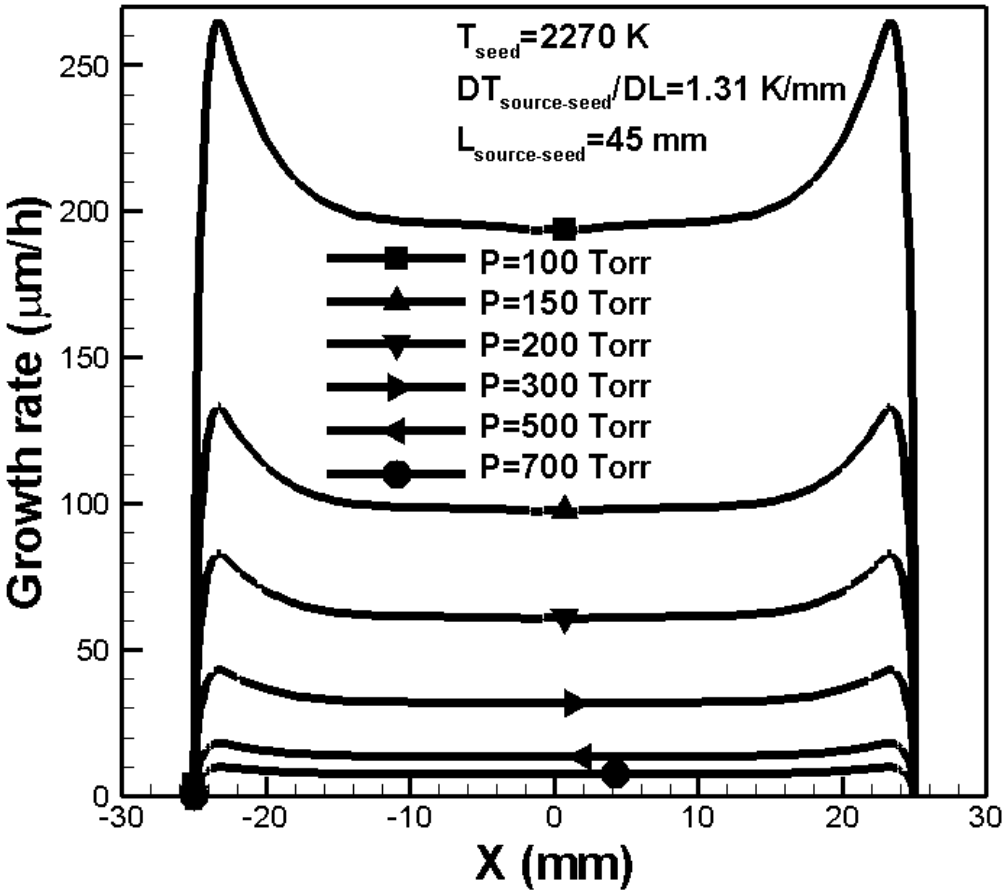
T_seed=2270 K
DT_source-seed/DL=1.31 K/mm
L_source-seed=45 mm
P=100 Torr
P=150 Torr
P=200 Torr
P=300 Torr
P=500 Torr
P=700 Torr
Growth rate (μm/h)
X (mm)
0
50
100
150
200
250
-30
-20
-10
0
10
20
30

Fig. 4(b).

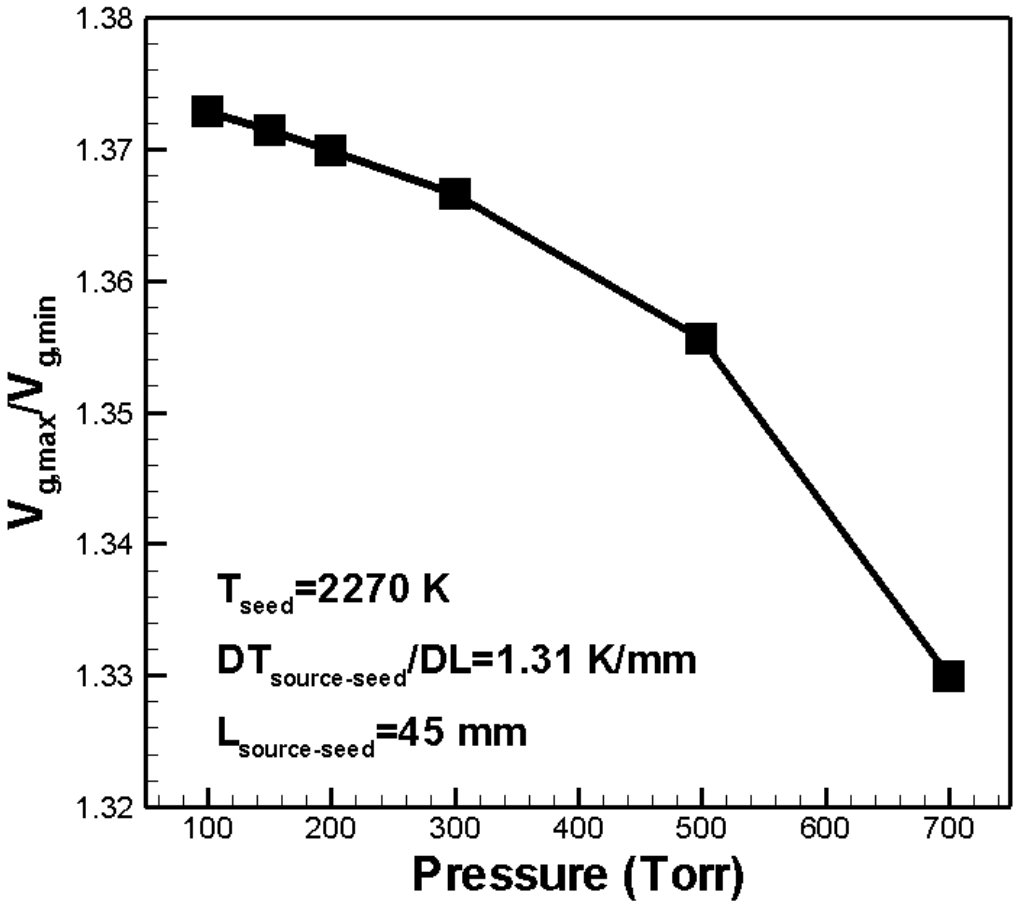
1.38
1.37
1.36
1.35
1.34
1.33
1.32
$V_{g,max}/V_{g,min}$
T_{seed}=2270 K
$DT_{source-seed}/DL$=1.31 K/mm
$L_{source-seed}$=45 mm
100
200
300
400
500
600
700
Pressure (Torr)

Fig. 5.

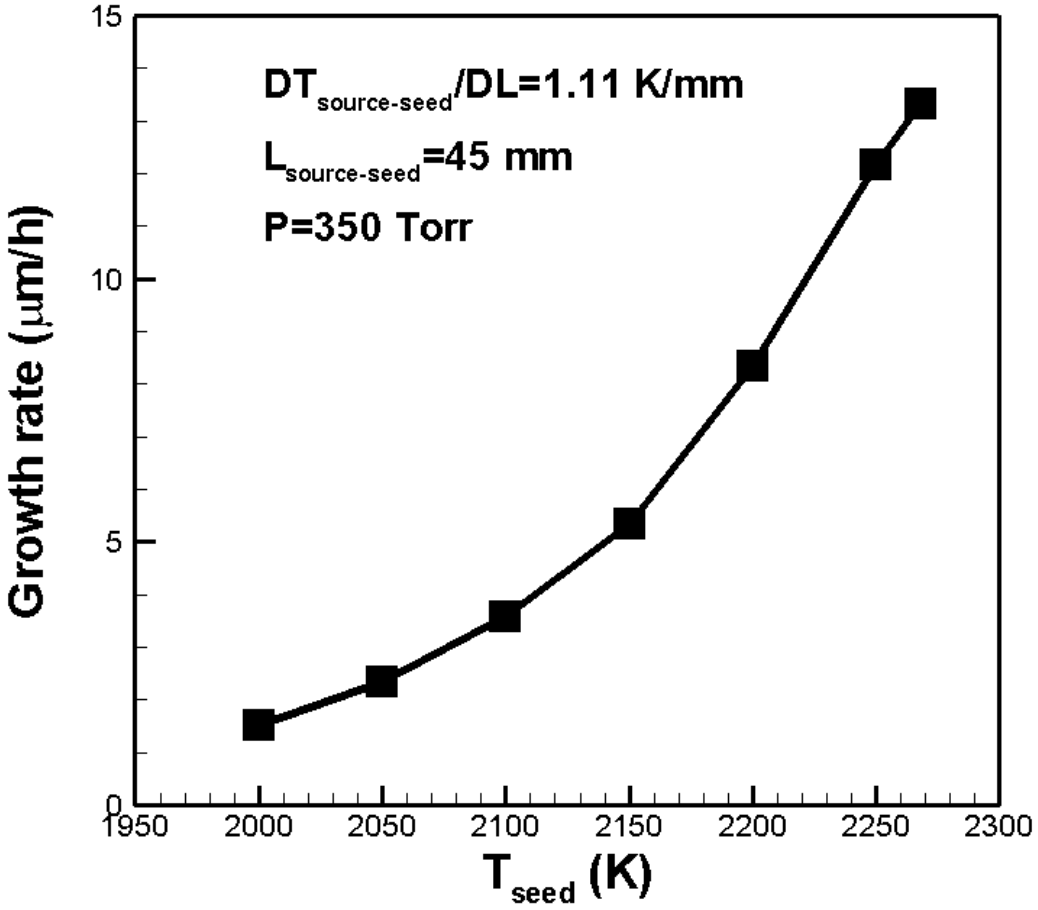
DT source-seed/DL=1.11 K/mm
L source-seed=45 mm
P=350 Torr
Growth rate (μm/h)
T seed (K)
0
5
10
15
1950
2000
2050
2100
2150
2200
2250
2300

Fig. 6.

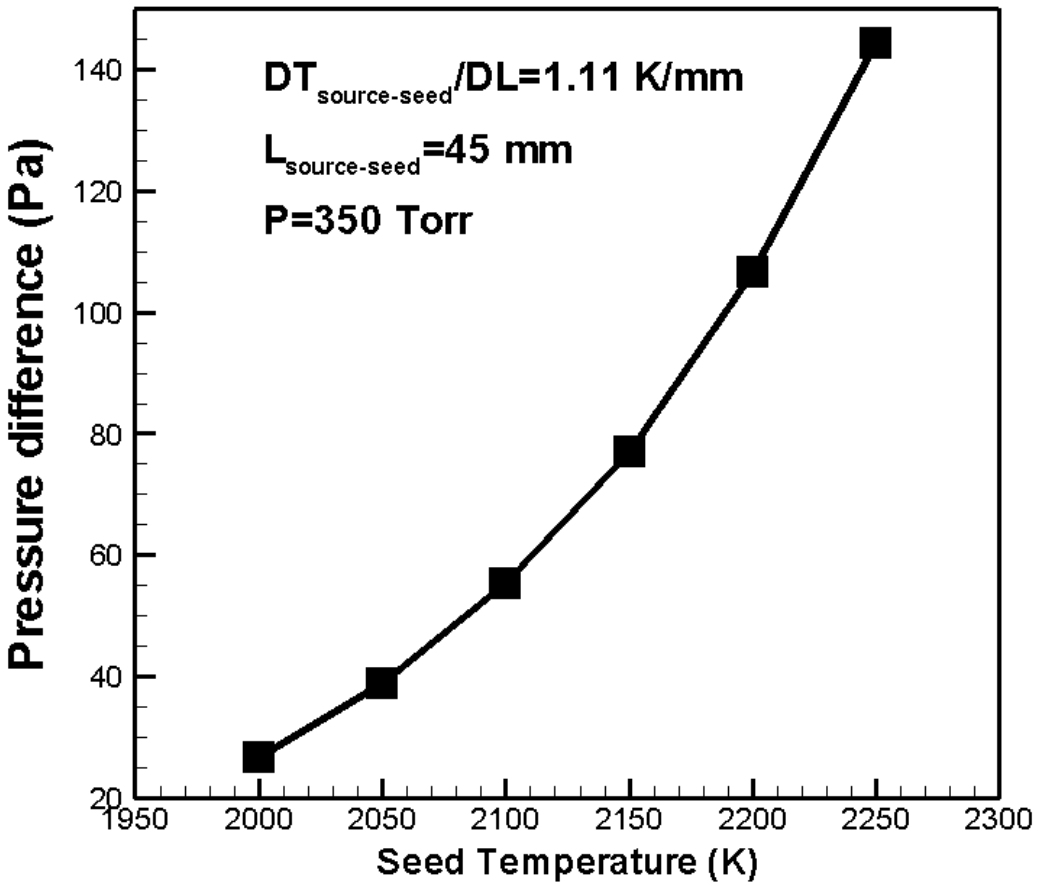
DT source-seed/DL=1.11 K/mm
L source-seed=45 mm
P=350 Torr
Pressure difference (Pa)
Seed Temperature (K)
20
40
60
80
100
120
140
1950
2000
2050
2100
2150
2200
2250
2300

Fig. 7.

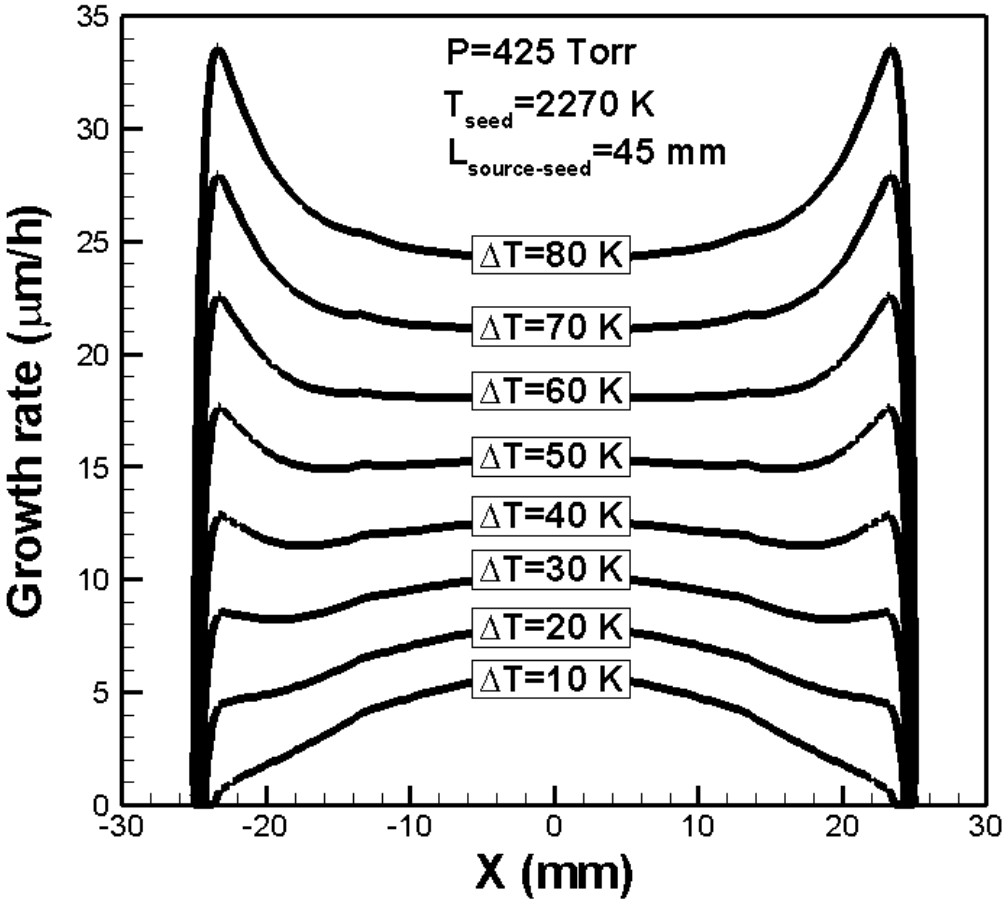
P=425 Torr
T_seed=2270 K
L_source-seed=45 mm
ΔT=80 K
ΔT=70 K
ΔT=60 K
ΔT=50 K
ΔT=40 K
ΔT=30 K
ΔT=20 K
ΔT=10 K
Growth rate (μm/h)
X (mm)
0
5
10
15
20
25
30
35
-30
-20
-10
0
10
20
30

Fig. 8.

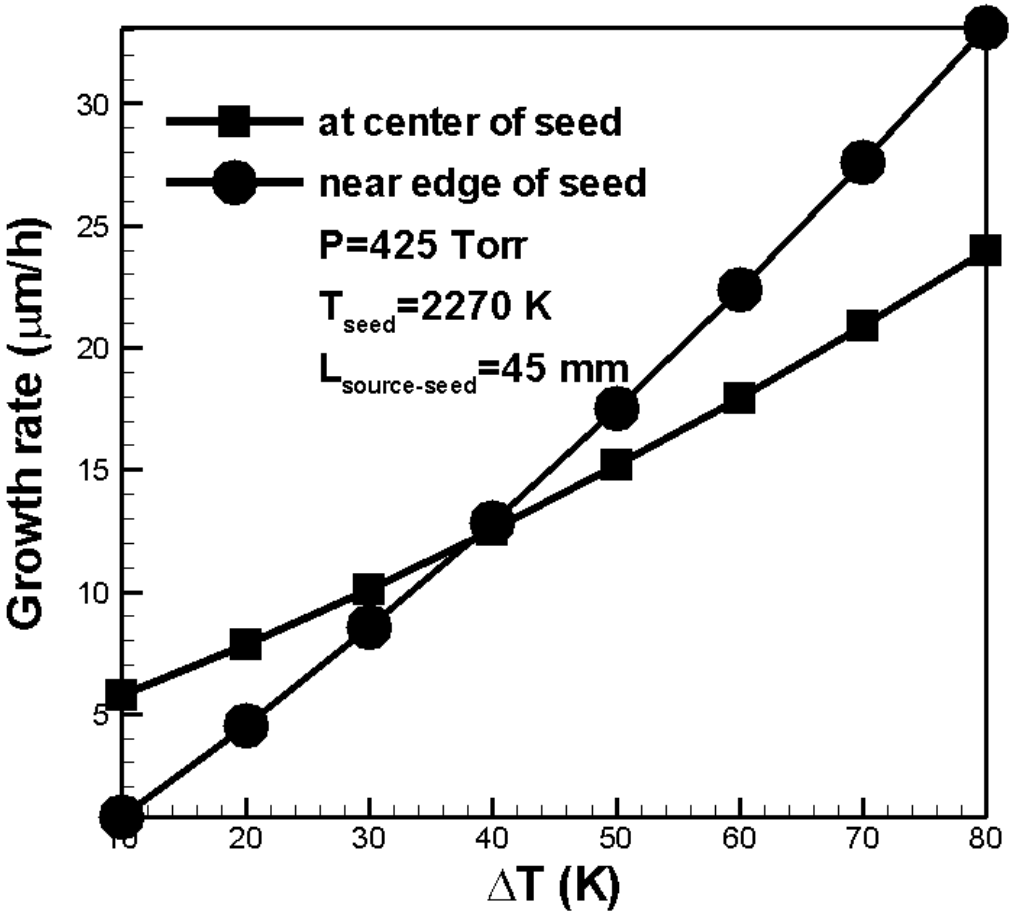
at center of seed
near edge of seed
P=425 Torr
T_seed=2270 K
L_source-seed=45 mm
Growth rate (μm/h)
ΔT (K)
5
10
15
20
25
30
20
30
40
50
60
70
80